Solid State Communications 149 (2009) 1403–1409

Contents lists available at ScienceDirect

Solid State Communications

journal homepage: www.elsevier.com/locate/ssc

Kinetic frustration of Ostwald ripening in Ge/Si(100) hut ensembles

Michael R. McKay [a], J.A. Venables [b,c], Jeff Drucker [b,d,*]

[a] Science and Engineering of Materials, Arizona State University, Tempe, AZ, 85287, USA
[b] Department of Physics, Arizona State University, Tempe, AZ, 85287, USA
[c] London Centre for Nanotechnology, University College, London, WC1H 0AH, United Kingdom
[d] School of Materials, Arizona State University, Tempe, AZ, 85287, USA

ARTICLE INFO

Article history:
Received 6 February 2009
Accepted 27 April 2009 by the Guest Editors
Available online 20 May 2009

PACS:
68.55.-a
81.15.Aa
61.46.Hk

Keywords:
A. Nanostructures
A. Surfaces and interfaces
B. Crystal growth
B. Epitaxy

ABSTRACT

We show that low area density Ge/Si(100) island ensembles comprised solely of hut and pyramid clusters do not undergo Ostwald ripening during days-long growth temperature anneals. In contrast, a very low density of large, low chemical potential Ge islands reduce the supersaturation causing the huts and pyramids to ripen. By assuming that huts lengthen by adding single {105} planes that grow from apex-to-base, we use a mean-field facet nucleation model to interpret these experimental observations. We find that each newly completed plane replenishes the nucleation site at the hut apex and depletes the Ge supersaturation by a fixed amount. This provides a feedback mechanism that reduces the island growth rate. As long as the supersaturation remains high enough to support nucleation of additional planes on the narrowest hut cluster, Ostwald ripening is suppressed on an experimental time scale.

© 2009 Elsevier Ltd. All rights reserved.

1. Introduction

The nanoscale 3D islands that spontaneously form at the early stages of semiconductor heteroepitaxy have attracted intense scrutiny in recent years. These structures are promising for technological application and provide fascinating insight into the atomic processes of crystal growth on surfaces. Many systems grow via the Stranski–Krastanov mode for which initially planar growth transforms into an islanded morphology. Evolution continues after the islanding transition as the initially defect-free islands grow, change shape and eventually dislocate. This evolution is in response to thermodynamic driving forces, subject to kinetic constraints. Some growth conditions result in apparently stable island ensembles with remarkably uniform sizes, implying that heteroepitaxy may provide a facile route to self-assembly of semiconductor quantum dots with nearly identical optical and electronic properties. In contrast, similar growth conditions can produce ensembles with non-uniform island sizes, shapes or compositions. The question then arises: Is it possible to understand the mechanisms of heteroepitaxial self-assembly well enough to produce island ensembles with desirable morphologies and properties? This question thematically links much of the work investigating these systems and has provoked continuing, sometimes spirited discussion.

In this contribution, we discuss the Ge/Si(100) system, which is a useful prototype for investigating semiconductor heteroepitaxy. By virtue of its lower surface energy, Ge initially wets Si(100) growing in layers to a kinetically determined thickness [1,2] greater than 3 ML (1 ML is a film 1 atom thick $= 6.78 \times 10^{14}$ atoms/cm^2 for the Si(100) surface). The first islands that form above this wetting layer are defect-free. The smallest are rectangular-based huts [3] or square-based pyramids [4] that are bound by shallow {105} facets that contact the (100) surface at ∼11°. As the islands grow, it may become energetically favorable to transform into multifaceted dome clusters with approximately octagonal bases bound by steeper, ∼25° facets [5]. Continued growth may lead island to dislocation [6] at a size analogous to the critical thickness for dislocation of planar epilayers.

Each of these island transitions results from a competition between surface and elastic energies and each 'shape' is described by distinct functional forms of the free energy and chemical potential [7,8]. Coexistence of differently shaped islands can dramatically affect ensemble evolution and complicate interpretation of experimental results. This was realized early on and shown to be responsible for the dramatic acceleration of the island growth rate

* Corresponding address: Department of Physics, Arizona State University, POB 871504, Tempe, AZ, 85287-1504, USA. Tel.: +1 480 965 9658; fax: +1 480 965 7954.
E-mail address: jeff.drucker@asu.edu (J. Drucker).

0038-1098/$ – see front matter © 2009 Elsevier Ltd. All rights reserved.
doi:10.1016/j.ssc.2009.04.047

observed when coherent islands dislocate [7]. More recently, experimental observations of 'anomalous coarsening' have been attributed to similar effects [8].

Both thermodynamic and kinetic arguments have been offered to explain the existence of island ensembles with narrow size distributions. The thermodynamic viewpoint suggests that there is an equilibrium size at which the island free energy is a minimum for a given shape [9,10]. Alternative descriptions suggest that there are island size dependent kinetic limitations that cause larger islands to grow more slowly than smaller islands leading to the experimentally observed behavior [11,12]. A useful method to clarify the situation is to perform annealing experiments. The existence of an equilibrium island size would be revealed during an annealing experiment by collapse of the island size distribution to the thermodynamically preferred size. Similarly, a kinetic growth limitation would be revealed by the more rapid growth of smaller islands leading to a narrowing of the island size distribution. The absence of either an equilibrium island size or a size dependent kinetic limitation to island growth might be revealed during an annealing experiment by Ostwald ripening.

Ostwald ripening is often observed during island growth and annealing experiments [6,13–15]. For islands growing on a planar substrate, Ostwald ripening is a surface diffusion mediated coarsening process driven by differences in the island chemical potential, μ. In a mean-field description, critical clusters are those with $\mu = \mu_c$, the system supersaturation. Those with $\mu < \mu_c$ grow while those with $\mu > \mu_c$ shrink and eventually dissolve. As the anneal progresses, μ_c shrinks, the critical cluster size grows and the ensemble coarsens. The mean island size increases and the supersaturation decreases with time according to a power laws with the exponents set by the rate limiting step for island growth. This description has been extended to include coexistence of islands with distinct functional forms of the chemical potential [7,8].

For the growth temperature annealing experiments described here, the deposition flux is terminated, but sample heating continues. Initially, the supersaturation is high and existing islands grow, decreasing the supersaturation. Eventually, the supersaturation may decrease so that μ_c is less than that of the island with the largest chemical potential and Ostwald ripening initiates. Here we describe two scenarios. The first follows that described above and we observe Ostwald ripening of hut and pyramid clusters suggesting the absence of an equilibrium hut or pyramid size [15]. In the second, Ostwald ripening is not observed, but we do not detect a narrowing of the island size distribution [16]. This observation suggests that there is no inherent kinetic limitation to island growth and that the lack of Ostwald ripening is due do some other effect. We present a simple mean-field rate equation description of facet nucleation that describes this behavior. This description may be general for a class of epitaxial nanostructures that grow by a facet nucleation mechanism. Prior to outlining this model of island growth, we describe the experiments and then present and discuss our results. Finally, we conclude and briefly discuss the generality of our model.

2. Experimental methods

We used real-time, *in situ* scanning tunneling microscopy (STM) to image Ge/Si(100) island ensembles during prolonged growth temperature anneals. The base pressure of the ion pumped system was 1.5×10^{-10} Torr. We found that leaving the resistively heated samples at the growth temperature for ~12 h subsequent to degassing but prior to cleaning by flash desorption of the native oxide minimized thermal drift. The Ge islands were grown using gas-source molecular beam epitaxy by admitting a pressure of $\sim 10^{-7}$ Torr digermane (Ge_2H_6) leading to growth rates in the 0.1–0.2 ML/min range. Ge deposition was terminated by closing the leak valve and the chamber pressure rapidly dropped to 1×10^{-9} Torr in 2 min. The samples were continuously imaged throughout the anneal. Ge coverages were measured using Rutherford backscattering spectrometry. We also imaged the samples using scanning electron microscopy to assess long-range uniformity of the island ensembles at length scales inaccessible to STM. Table 1 summarizes the growth parameters for the samples discussed here.

Table 1
Sample growth parameters. T is the substrate temperature, R is the deposition rate and θ_{Ge} is the Ge coverage.

Sample	T (°C)	R (ML/min)	θ_{Ge}(ML)	Comments
A	450	0.1	5.0	Non-ripening
B	400	0.1	3.6	Non-ripening
C	500	0.1	5.6	Ripening
D	400	0.1	6.0	Ripening

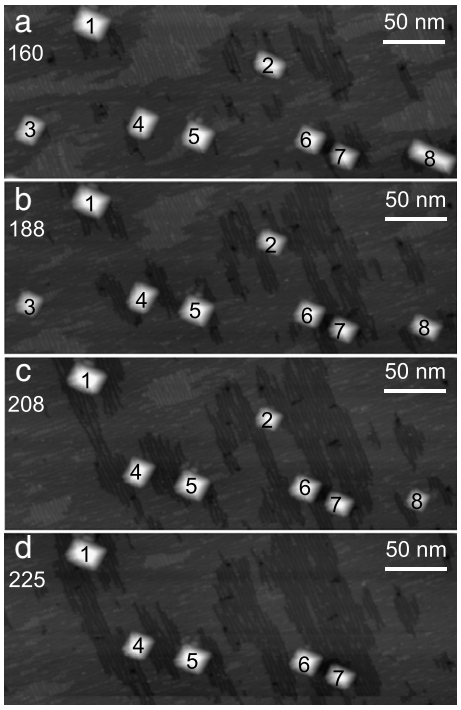

Fig. 1. A sequence of 360 nm × 140 nm STM images of sample C acquired at the indicated annealing times in minutes. Sample C was grown and annealed at $T = 500$ °C. Ostwald ripening is clearly evident as islands 2, 3 and 8 all dissolve by 225 min of annealing time.

3. Results and discussion

We first discuss samples C and D for which we observed Ostwald ripening. Following that discussion, we contrast these results with those of samples A and B for which no Ostwald ripening was observed. Fig. 1 shows a sequence of 360 nm × 140 nm STM images grabbed at the indicated times in minutes relative to the termination of Ge deposition from the STM movie acquired during the anneal of sample C, which was grown and annealed at $T = 500$ °C. The entire STM movie, encompassing the entire 14 h anneal is available online [17]. The growth conditions employed produced mixed hut and pyramid ensembles, as evident in Fig. 1(a). Fig. 1(b)–(d) display the same substrate region displayed in Fig. 1(a) at later annealing times. It is evident from this image sequence that the ensemble ripens, resulting in the complete dissolution of islands 2, 3 and 8.

The STM images allow access to the island length (L), width (W) and volume (V) as a function of time. We observe that the most common ripening pathway is for the narrowest hut

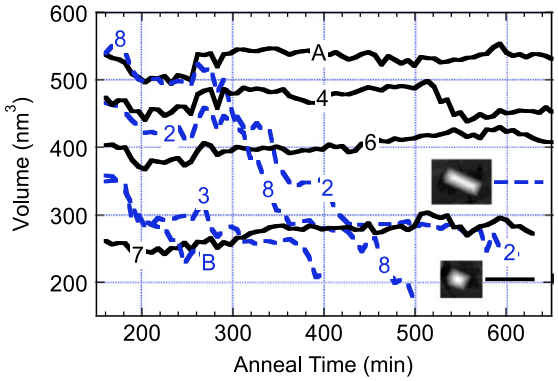

Fig. 2. Evolution of island volume for selected islands in sample C. Solid lines denote islands that do not shrink during the displayed time interval. Dashed lines indicate islands that shrink during the displayed time interval. Curves are labeled with numbers that correspond to the island numbers displayed in Fig. 1. Curves 'A' and 'B' correspond to islands not displayed in Fig. 1. The initial volumes and widths of these islands are tabulated in Table 2.

Table 2
Initial volume and width of islands plotted in Fig. 1.

Island	V_o (nm^3)	W (nm)
A	540	24
B	450	17
2	480	21
3	300	21
4	390	24
6	500	23
7	250	20
8	360	19

clusters to reduce their length at fixed width. Interestingly, island width, rather than volume, appears to be the parameter that determines whether an island grows or dissolves. This observation is substantiated by Fig. 2 and Table 2. Fig. 2 displays island volume as a function of anneal time for selected islands and Table 2 indicates the starting volumes and widths of these islands. Evidently, the narrowest islands (B, 2, 3 and 8) all shrink while the wider islands (A, 4, 6 and 7) do not. Island 7 is an exception and below we argue that this is likely due to an elastic interaction with island 6. At the early stages of the anneal, islands with $W \leq 21$ nm continuously shrink, while those with larger W grow slowly, suggesting that there is a W above which hut clusters are stable for these annealing conditions. We find that this critical W increases throughout the anneal so that after about 10 h of annealing, islands with $W \leq 25$ nm are no longer stable.

While some of the hut clusters evident in the STM field of view slowly grow throughout the anneal, their volume increase is not sufficient to account for those that dissolve. *ex situ* scanning electron microscopy indicates that a very low density of $3 \times 10^5/\text{cm}^2$ of very large, $\sim 1\,\mu$m diameter clusters are responsible for the decrease in volume of the hut/pyramid ensemble. Presumably, these clusters are highly defective and relaxed and therefore have a low chemical potential [6]. Thus, we believe that they serve as effective sinks for diffusing Ge dimers and reduce the supersaturation, destabilizing the hut/pyramid ensemble to Ostwald ripening. This proposal is supported by observation of a $\sim$400 nm wide denuded zone devoid of any huts or pyramids surrounding these large clusters [15].

As discussed in Ref. [15], very similar behavior was observed for sample D, which was grown and annealed at $T = 400\,^\circ$C. As expected, the ripening kinetics were slower at this temperature, but the qualitative behavior observed was very similar to that for sample C. W rather than V once again appears to be the parameter that determines island stability. Also, large clusters at a density

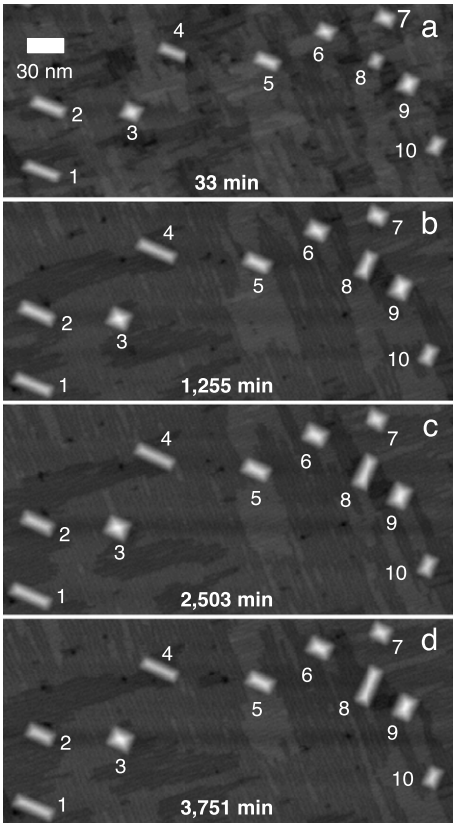

Fig. 3. A sequence of 360 nm $\times$ 160 nm STM images of sample A acquired at the indicated anneal times in minutes. Sample A was grown and annealed at $T = 450\,^\circ$C. This sample exhibits no signs of Ostwald ripening. Note that all islands grow and that wetting layer features coarsen.

of $8 \times 10^3/\text{cm}^2$ play the same role in destabilizing the hut and pyramid ensemble to Ostwald ripening. A substantive difference between samples C and D is that for the sample grown and annealed at the lower temperature, we do not observe a denuded zone around the large clusters. We attribute this final observation to reduced surface diffusion at the lower temperature.

We now turn our attention to samples A and B, which were grown using conditions similar to samples C and D but to lower Ge coverages and exhibited no signs of Ostwald ripening. Using *ex situ* SEM, we found that the entire 3×20 mm surfaces of samples A and B were devoid of the large clusters found at low density on samples C and D and were populated solely by huts and pyramids. In what follows, we discuss sample A in detail, but the behavior observed for sample B was very similar except for the reduced kinetics due to the lower growth and annealing temperature. Fig. 3 displays a sequence of 360 nm $\times$ 160 nm STM images of the same area of sample A grabbed from a sequence of 600 nm $\times$ 600 nm images available online in movie format [17]. In contrast to the behavior of samples C and D, we observe no signs of Ostwald ripening. Rather, all clusters grow, more rapidly initially, suggesting that they all remain above the critical size for Ostwald ripening throughout the anneal. We also find that in most cases, the huts grow by increasing their length but not their width. Also evident in Fig. 3 is a decreasing height modulation in the wetting layer as the anneal progresses. While it is difficult to quantify, due to the relatively few gray levels associated with the few-ML height modulations, we believe that this signifies decreasing free Ge concentration that feeds growth of the hut ensemble as the anneal progresses. Importantly, we do not observe the wetting layer surface reconstruction to change, suggesting that its composition is relatively static. But we do observe significant

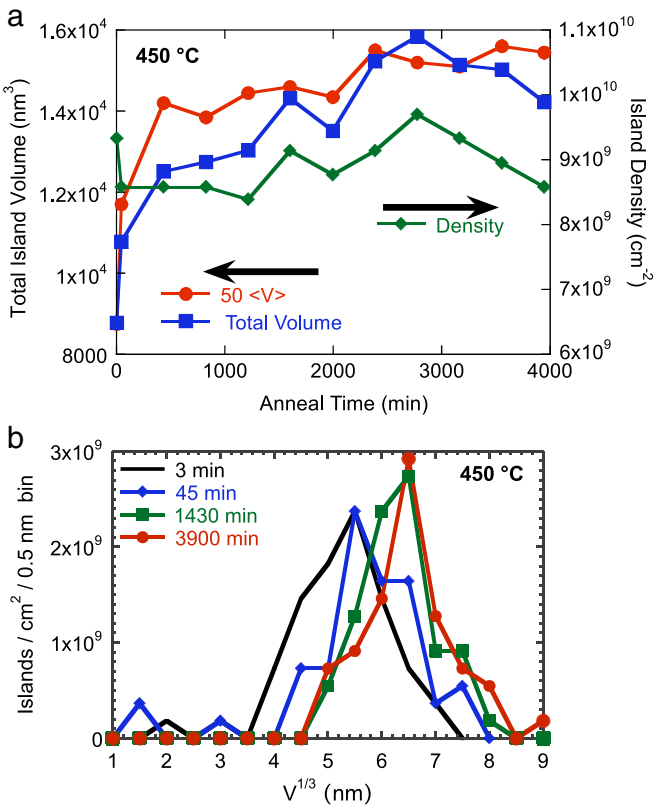

Fig. 4. (a) Total island volume, average island volume and island density vs. anneal time and (b) evolution of island volumes vs. anneal time for the sample displayed in Fig. 3.

coarsening of 2D features indicating significant surface diffusion throughout the anneal.

The absence of Ostwald ripening is quantified in Fig. 4. Fig. 4(a) summarizes the evolution of island volume and density. Fig. 4(b) displays the evolution of the island volume distribution during the anneal. Evident in Fig. 4(a) is a relatively rapid increase in island volume at the early stages of the anneal followed by a slower increase. Fluctuations in the total and average island volume can be quantitatively accounted for by islands moving into or out of the STM field of view during the anneal due to thermal drift. Contrary to what would be expected for Ostwald ripening, none of the islands dissolves and the island density is constant. Fig. 4(b) shows that the island volume distribution does not change appreciably, particularly at long anneal times. The shift to larger volumes between 3 and 1430 min correlates with increase in island volume evident during that time range in Fig. 4(a). There is almost no change in the volume distribution for $1430 > t > 3900$ min.

We believe that Fig. 4 suggest the absence of a size-dependent kinetic growth limitation and that the observation of Ostwald ripening in samples C and D indicate the lack of a thermodynamically preferred island size. If there were a thermodynamically preferred size, then it would be manifested by collapse of the island size distribution to that size during the anneals. Existence of a size-dependent kinetic growth limitation, similar to those previously proposed, [11,12] would cause smaller islands to grow more rapidly than larger islands and the island size distributions of Fig. 4(b) would obviously narrow. We do not observe behavior suggestive of either a thermodynamically preferred island size or a size-dependent kinetic growth limitation. Rather, we observe Ostwald ripening in the presence of large clusters and diminishing growth during the anneal in the absence of large clusters. In the former case, the large clusters serve to reduce the Ge supersaturation and destabilize the hut and pyramid ensemble to Ostwald ripening. In the absence of the large clusters, the only avenue for reducing the Ge supersaturation is via growth of the hut clusters. We believe that this reduction of the Ge supersaturation is responsible for the experimentally observed decrease of the island growth rate displayed in Fig. 4(a). If this island growth rate is too slow, then the Ge supersaturation cannot reduce to the level required to initiate Ostwald ripening on an experimental time scale.

We believe that our experimental observations can be explained using the following model. Similar to previous descriptions of hut and pyramid cluster growth, we assume that the clusters grow by adding single {105} planes [11,12]. Contrary to those models, we assume the new planes nucleate at the cluster apex where the elastic energy density is the lowest, and grow toward the base, following the scenario depicted in the inset of Fig. 6. Supporting our proposal is the observation that, at least during the pyramid-to-dome transition, additional {105} planes grow from apex-to-base [18]. Since we never observe incomplete facets, we assume that stable nuclei grow rapidly to completion and that nucleation of new planes is the rate-limiting step in island growth. The following sequence of events conspire to allow the hut growth rate to fall to nearly zero during the anneal.

First, each newly completed plane 'replenishes' the nucleation site at the cluster apex, making it available for another nucleation event. This guarantees a constant density of nucleation centers. Since the huts grow primarily by increasing their length, and their widths remain nearly constant, the end facet size and chemical potential distributions are essentially static. Thus, the decreasing Ge supersaturation is the only pathway to Ostwald ripening. Finally, each completed plane depletes the Ge supersaturation by a set amount, providing a feedback mechanism that reduces the nucleation rate and the island growth rate. As long as the remaining supersaturation supports a critical nucleus size smaller than the number of dimers comprising the smallest end facet, Ostwald ripening is suppressed.

Our strategy to model this sequence of events starts with finding the supersaturation-dependent facet nucleation rate. We then connect this nucleation rate to the island growth rate and reduction of Ge supersaturation to demonstrate a diminishing island growth rate as the anneal progresses.

We begin by considering the (2D facet) embryo formation energy, $E_f = E_s + \Delta E_{el}$ using the geometry depicted in the Fig. 6 inset. $E_s = r\,(2\Gamma_e + \theta\Gamma_s)$ is the step/edge contribution. r is the radius of the circular-section embryo, θ is the apex angle of the {105} facet $\cong \pi/2$, Γ_s is the {105} step energy ≈ 0.12 eV/nm, [18,19] and Γ_e is the specific edge energy at the junction of adjacent {105} planes. The elastic contribution, $\Delta E_{el} = E_{el,f} - E_{el,WL}$, is found by finite element methods. The finite element model employed periodic boundary conditions in the growth plane. Empirically, we found that elastic interactions between neighboring pyramids were negligible if their edges were spaced by at least $2W$. We always chose the substrate depth to be $> W/2$ to ensure that the elastic distortions decayed sufficiently at the bottom of the simulation cell. We employed fully anisotropic elastic moduli and simulated {105} faceted Ge pyramids atop a 3 ML thick Ge wetting layer on a Si(100) substrate.

Results are summarized in Fig. 5. Fig. 5(a) displays the elastic energy density in J/m^3 at the surface of a pyramid cluster with side length, $W = 10$ nm. Fig. 5(b) plots the elastic energy density for pyramids with the indicated widths along lines passing down the center of a facet or along the edge joining adjacent facets. $E_{el,f}$ is the embryo strain energy and $E_{el,WL}$ is the elastic energy of the same amount of Ge in the biaxially strained wetting layer. For $E_{el,f}$, we find that the volume elastic energy density increases linearly away from the pyramid apex for the upper 80% of the facet, as shown in Fig. 5(b). Thus, the elastic energy of an embryo growing at the

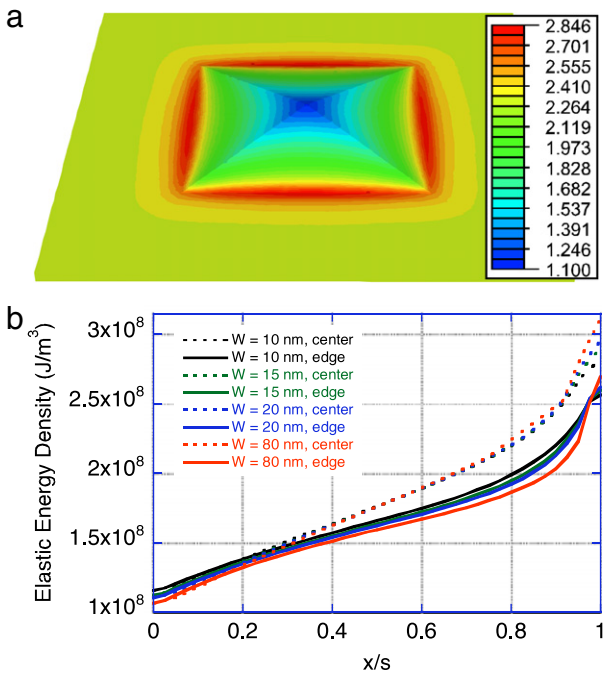

Fig. 5. (a) Elastic energy density in J/m^3 at the surface of a 10 nm base width, {105} faceted Ge/Si(100) pyramid cluster. (b) Elastic energy density in J/m^3 vs. scaled distance from the apex for pyramids of the indicated base widths along lines passing down either the center of one of the {105} facets or along the edge at the junction of adjacent {105} facets. $x = 0$ corresponds to the pyramid apex and $s = W/2$. Note that the elastic energy density varies linearly along the upper 80% of the facet and that it does not vary significantly for pyramids in the relevant size range.

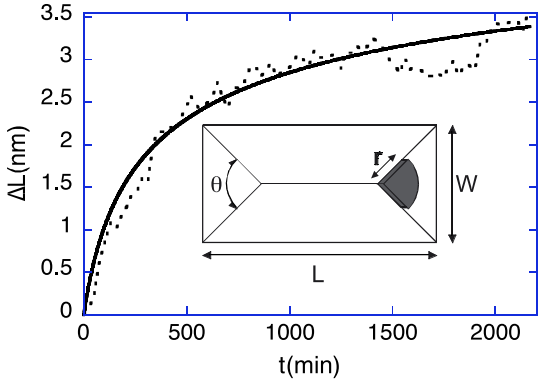

Fig. 6. Comparison between experiment (dashed line) and model (solid line). Experimental curve is the average change in length, ΔL, for the 34 huts that remain in the STM field of view for during the time interval on the horizontal axis. The inset shows the geometry used in the model.

cluster apex is

$$E_{el,f} = \alpha h\theta r^2/2 + \beta h\theta \cos\gamma r^3/(3s) \tag{1}$$

with $\alpha = 0.7$ eV/nm^3 and $\beta = 0.81$ eV/nm^3. Fig. 5(b) also shows that α and β do not vary significantly for huts in the relevant size range. $h = 0.053$ nm is the {105} plane spacing, which is the embryo thickness, $\gamma = 11.3°$ is the contact angle of the {105} facet to the (100) substrate and $2s$ is the hut width. For s, we use the experimentally measured average of 5.6 nm. The finite element model also finds that the elastic energy density of the wetting layer, $dE_{el,WL}$ is 1.44 eV/nm^3, the same 30 meV/atom value found in Ref. [20].

The free energy change upon formation of an embryo comprised of j dimers is $\Delta G(j) = E_f - j\Delta\mu$. Since $j = (\sigma_d\theta/2)\, r^2$,

$$\Delta G(j) = Xj^{1/2} + (A - \Delta\mu)\, j + Bj^{3/2}. \tag{2}$$

$\sigma_d = 1.33$ dimers/nm^2 is the dimer density of a {105} plane [18] and $\Delta\mu$ is the Ge dimer supersaturation that drives island growth. A, B and X are constants defined by material parameters:

$$X = (2\Gamma_e + \theta\Gamma_s)\sqrt{2/(\theta\sigma_d)} \tag{3a}$$

$$A = (\alpha h)/\sigma_d - dE_{el,WL} \tag{3b}$$

$$B = \frac{\beta h\cos\gamma}{3s}\sqrt{\frac{8}{\theta\sigma_d^3}}. \tag{3c}$$

Maximizing $\Delta G(j)$ gives the facet nucleation barrier, $\Delta G(i)$, where i is the number of dimers in the critical nucleus:

$$\Delta G(i) = \frac{1}{27B^2}\left[C\left(9BX - 2C^2\right) + 2\left(C^2 - 3BX\right)^{3/2}\right] \tag{4a}$$

$$i = \frac{1}{9B^2}\left[2C^2 - 3BX - 2C\sqrt{C^2 - 3BX}\right] \tag{4b}$$

with $C = \Delta\mu - A$.

It has been suggested that an additional energy barrier must be surmounted to form stable nuclei on reconstructed surfaces [21] and this effect significantly modifies 2D growth on Si(111)-7×7 [22]. The rebonded step (RS) reconstruction [23–25] found on {105} hut facets is complex with significant distortion relative to the bulk [26]. Cereda and Montalenti [27] found an 0.5 eV barrier must be overcome to remove the RS reconstruction and incorporate 7 Ge atoms into a new layer on the Ge(105) surface. Thus, we include an additional 0.5 eV into $\Delta G(i)$ for nuclei with $i \geq 3.5$ dimers. i and $\Delta G(i)$ provide input into a mean field description of facet nucleation that can predict the island growth rate.

The nucleation rate of new stable facets is $U_n = A_f Z\sigma_i D n_1 n_i$. $n_i = n_1 e^{-\Delta G(i)/kT}$ is the density of critical nuclei, A_f is the average facet area $= s^2/\cos\gamma$ and Z is the Zeldovich factor [28]. σ_i is the capture number, which scales initially as the number of perimeter sites of a critical nucleus. The diffusion coefficient is $D = \nu/(4N_o)\, e^{-(E_d/kT)}$. $\nu = 5$ THz is a surface vibrational frequency, N_o is the area density of surface sites, $E_d = 1$ eV [29] is the Ge dimer diffusion activation energy and k is Boltzmann's constant. The density of diffusing Ge dimers, n_1, is related to the equilibrium dimer density, $n_1^e = N_o e^{-L_2/kT}$ ($L_2 = 0.3$ eV [30] is the dimer formation energy), through $\Delta\mu = kT\ln\left(n_1/n_1^e\right)$. Combining these expressions yields the production rate of stable {105} facets

$$U_n = 1/4 A_f Z\sigma_i \nu N_o e^{E_n/kT}. \tag{5}$$

where

$$E_n = 2(\Delta\mu - L_2) - [E_d + \Delta G(i)] \tag{6}$$

is a characteristic nucleation energy.

We can find the rate that the free Ge dimer population decreases by noting that there are 2 end facets per hut, $N = 8.5 \times 10^9$ huts/cm^2 and each new facet consumes $A_f\sigma_d$ dimers so that

$$\frac{dn_1}{dt} = -2NA_f\sigma_d U_n. \tag{7}$$

The hut growth rate is simply $dL/dt = 2U_n L_{105}$ where $L_{105} = 0.27$nm is the increase in hut length as a new {105} facet is added. Eqs. (5) and (7) are coupled differential equations that we numerically integrate to find the island growth rate, $\Delta\mu$, i and $\Delta G(i)$ as the anneal progresses.

Figs. 6 and 7 display results of our model. The only adjustable parameters are the starting Ge supersaturation and edge energy, Γ_e. Fig. 6 compares the growth rate of an average-sized hut to the average growth rate of the 34 islands that remain in the STM field of view during the displayed time interval. The standard deviation of the experimentally measured average ΔL is about 1nm. We believe that it arises from variations in the local chemical potential

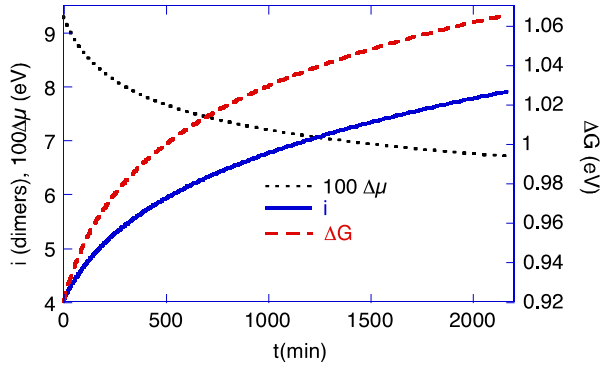

Fig. 7. Supersaturation $\Delta\mu$, critical nucleus size i and facet nucleation barrier $\Delta G(i)$ vs. annealing time t. $\Delta\mu$ falls during the anneal, slowing the island growth rate but i remains smaller than the smallest end facet size so that Ostwald ripening is suppressed.

and spatial correlations between the islands that are not captured by our mean-field model. The starting $\Delta\mu$ was chosen so that sufficient Ge is available to support the experimentally observed island growth. The fit shown in Fig. 6 was for an initial dimer density satisfying $n_1/n_1^e = 4.45$ giving an initial supersaturation of 93 meV/dimer. Here, we set $\Gamma_e = \Gamma_s$ and will explore the consequences of varying Γ_e in a later publication.

Fig. 7 displays the time evolution of $\Delta\mu$, i and $\Delta G(i)$. Note that although i steadily increases during the anneal, its maximum value, $i \cong 8$ dimers, is much less than the number of dimers comprising the end facet of the smallest hut cluster. An end facet consisting of only 8 dimers would have $s = 2.5$ nm and the smallest we observed was about twice this large. Even at the end of the anneal, the supersaturation is high enough so that all facets are supercritical and Ostwald ripening is suppressed. The decrease of $\Delta\mu$ is responsible for the reduced island growth rate evident in Fig. 6.

We now briefly discuss application of this facet nucleation description of kinetic hut stability to samples C and D for which Ostwald ripening was observed. As discussed above, these samples differ from samples A and B for which we did not observe Ostwald ripening in that they both exhibited a low density of large, low μ clusters that served as sinks for Ge and reduced the supersaturation. Apparently, the behavior exhibited by these samples is described by the limit in which the system supersaturation is not large enough to support a critical nucleus size smaller than the smallest end facet. In this case, huts with small end facets cannot grow by the facet nucleation mechanism described by our model and decrease in length as experimentally observed. The lone exception is island 7 in Fig. 1. We believe that the reason this island does not shrink during the anneal even though its width is less than the 'critical' width of 21 nm (see Table 2) at the beginning of the anneal is due to the proximity of island 6. These islands are close enough to interact elastically, and such interactions can influence ripening kinetics. [31]

Finally, we note that the criterion for successful nucleation of a new {105} plane is that the chemical potential of the completed facet (i.e., the underlying facet the new plane is growing upon) is less than the supersaturation. This is exactly the stability condition determining whether or not the ensemble of {105} end facets is stable or unstable with respect to Ostwald ripening. Essentially, our facet nucleation description of hut growth and kinetic stability simply recasts the problem of hut/pyramid ensemble stability into the problem of stability of the ensemble of end {105} facets. We believe that it is reasonable to do so since the chemical potential of the side facets of the hut clusters is less than that of the end facets and simple estimates of the chemical potential of the entire hut cluster show that it is far smaller than that of the end facet.

Our kinetic stability model is general, and should apply to any system with a constant density of replenishable nucleation centers producing facets that do not grow much in size. This is clearly satisfied for Ge/Si(100) hut clusters and should be satisfied for, e.g., metal silicide nanowires [32]. Whether or not similar arguments could apply to more complex, multifaceted structures such as domes or the Ge pyramid analogs found in InAs/GaAs(100) that are bound by {137} facets [33] is not clear and invites further experimental and theoretical investigation.

4. Summary and conclusion

In summary, we have found that low area density Ge/Si(100) hut ensembles can be kinetically stabilized during prolonged annealing at the growth temperature. This behavior is observed only if there are no lower chemical potential islands that reduce the Ge supersaturation and initiate Ostwald ripening. We explain this behavior using a model that shows diminished hut growth is a consequence of falling Ge supersaturation. The falling Ge supersaturation, in turn, dramatically reduces the rate that new facets nucleate providing a feedback mechanism allowing the hut growth rate to fall to nearly zero. Ostwald ripening is suppressed as long as the critical nucleus size is smaller than the smallest hut facet. In contrast, if the supersaturation drops below that required to drive nucleation on the smallest end facet in the hut cluster ensemble, Ostwald ripening occurs. Thus, our facet nucleation description interprets the kinetic stability of the hut cluster ensemble in terms of the kinetic stability of the ensemble of end facets.

Acknowledgements

This work was supported by the National Science Foundation. MRM was supported by an DOE Fellowship through Sandia National Laboratories.

References

[1] T. Walther, A.G. Cullis, D.J. Norris, M. Hopkinson, Phys. Rev. Lett. 86 (2001) 2381.
[2] Yuhai Tu, J. Tersoff, Phys. Rev. Lett. 93 (2004) 216101.
[3] Y. Mo, D.E. Savage, B.S. Swartzentruber, M.G. Lagally, Phys. Rev. Lett. 65 (1990) 1020.
[4] G. Medeiros-Ribeiro, T.I. Kamins, D.A. Ohlberg, R. Stanley Williams, Phys. Rev. B 58 (1997) 3533.
[5] M. Tomitori, K. Watanabe, M. Kobayashi, O. Nishikawa, Appl. Surf. Sci. 76/77 (1994) 322.
[6] M. Krishnamurthy, J. Drucker, J.A. Venables, J. Appl. Phys. 69 (1991) 6461.
[7] J. Drucker, Phys. Rev. B. 48 (1993) 18203.
[8] F.M. Ross, J. Tersoff, R.M. Tromp, Phys. Rev. Lett. 80 (1998) 984.
[9] V. Shchukin, N.N. Ledentsov, P.S. Kop'ev, D. Bimberg, Phys. Rev. Lett. 75 (1995) 2968.
[10] I. Daruka, A.-L. Barabási, Phys. Rev. Lett. 79 (1997) 3708.
[11] D. Jesson, G. Chen, K.M. Chen, S.J. Pennycook, Phys. Rev. Lett. 80 (1998) 5156.
[12] M. Kästner, B. Voigtländer, Phys. Rev. Lett. 82 (1999) 2745.
[13] T. Kamins, G. Medeiros-Ribeiro, D.A.A. Ohlberg, R. Stanley Williams, J. Appl. Phys. 85 (1999) 1159.
[14] Y. Zhang, J. Drucker, J. Appl. Phys. 93 (2003) 9583.
[15] M.R. Mckay, J. Shumway, J. Drucker, J. Appl. Phys. 99 (2006) 094305.
[16] Michael R. McKay, J.A. Venables, Jeff Drucker, Phys. Rev. Lett. 101 (2008) 216104.
[17] http://physics.asu.edu/jsdruck/stm_anneal.htm.
[18] F. Montalenti, P. Raiteri, D.B. Migas, H. von Känel, A. Rastelli, C. Manzano, G. Costantini, U. Denker, O.G. Schmidt, K. Kern, Leo Miglio, Phys. Rev. Lett. 93 (2004) 216102.
[19] S. Cereda, F. Montalenti, L. Miglio, Surf. Sci. 591 (2005) 23.
[20] J. Tersoff, Phys. Rev. B 43 (1991) 9377.
[21] R. Pala, F. Liu, Phys. Rev. Lett. 95 (2005) 136106.
[22] S. Filimonov, Vasily Cherepanov, Yuri Hervieu, Bert Voigtländer, Phys. Rev. B 76 (2007) 035428.
[23] K.E. Khor, S. Das Sarma, J. Vac. Sci. Technol. B 15 (1997) 1051.
[24] Y. Fujikawa, K. Akiyama, T. Nagao, T. Sakurai, M.G. Lagally, T. Hashimoto, Y. Morikawa, K. Terakura, Phys. Rev. Lett. 88 (2002) 176101.
[25] P. Raiteri, D.B. Migas, Leo Miglio, A. Rastelli, H. von Känel, Phys. Rev. Lett. 88 (2002) 256103.
[26] D.B. Migas, S. Cereda, F. Montalenti, Leo Miglio, Surf. Sci. 556 (2004) 121.

[27] S. Cereda, F. Montalenti, Phys. Rev. B 75 (2007) 195321.
[28] D.R. Frankl, J.A. Venables, Adv. Phys. 19 (1970) 409.
[29] X.R. Qin, B.S. Swartzentruber, M.G. Lagally, Phys. Rev. Lett. 85 (2000) 3660.
[30] T. Schwarz-Selinger, Y.L. Foo, David G. Cahill, J.E. Greene, Phys. Rev. B 65 (2002) 125317.
[31] J.A. Floro, M.B. Sinclair, E. Chason, L.B. Freund, R.D. Twesten, R.Q. Hwang, G.A. Lucadamo, Phys. Rev. Lett. 84 (2000) 701.
[32] Z. He, M. Stevens, D. Smith, P. Bennett, Surf. Sci. 524 (2002) 148.
[33] P. Kratzer, Q.K.K. Liu, P. Acosta-Diaz, C. Manzano, G. Costantini, R. Songmuang, A. Rastelli, O.G. Schmidt, K. Kern, Phys. Rev. B 73 (2006) 205347.